Journal of Computational Chemistry

Photoelectron Spectrum of NO_2^-: SAC-CI Gradient Study of Vibrational-Rotational Structures

Tomoo Miyahara, and Hiroshi Nakatsuji*

Three-dimensional accurate potential energy surfaces around the local minima of NO_2^- and NO_2 were calculated with the SAC/SAC-CI analytical energy gradient method. Therefrom, the ionization photoelectron spectra of NO_2^-, the equilibrium geometries and adiabatic electron affinity of NO_2, and the vibrational frequencies including harmonicity and anharmonicity of NO_2^- and NO_2 were obtained. The calculated electron affinity was in reasonable agreement with the experimental value. The SAC-CI photoelectron spectra of NO_2^- at 350 K and 700 K including the rotational effects were calculated using the Franck–Condon approximation. The theoretical spectra reproduced well the fine experimental photoelectron spectra observed by Ervin et al. (J. Phys. Chem. 1988, 92, 5405). The results showed that the ionizations from many vibrational excited states as well as the vibrational ground state are included in the experimental photoelectron spectra especially at 700 K and that the rotational effects are important to reproduce the experimental photoelectron spectra of both temperatures. The SAC/SAC-CI theoretical results supported the analyses of the spectra by Ervin et al., except that we could show some small contributions from the asymmetric-stretching mode of NO_2^-. © 2018 Wiley Periodicals, Inc.

DOI:10.1002/jcc.25608

Introduction

In the photoelectron spectra of NO_2^- at 350 K and 700 K reported by Ervin et al.,[1] the fine structures of the vibrational-rotational states were observed.[1] These high-resolution spectra provided the precise information of the geometrical structures, electronic properties, and vibrational and rotational spectroscopic constants. Ervin et al. carried out systematic analyses giving satisfactory explanations of the spectral details of the observed structures. We study here their fine photoelectron spectra in the light of the SAC/SAC-CI theoretical analyses.

The SAC/SAC-CI method[2–5] has been established for investigating molecular excited states through numerous applications in wide fields of chemistry and physics. The method has been applied to many subjects of molecular, biological, and surface photochemistry.[6–10] The SAC/SAC-CI analytical energy gradient method was formulated and implemented in 1997[11–13] and applied to the geometry optimizations of molecules in the ground, excited, ionized, electron attached, and high-spin states.[9,13] In the previous paper,[14] the low-lying valence singlet and triplet excited states of HAB molecules were investigated. The vibrational emission spectra of HSiF and DSiF and the absorption spectra of HSiCl and DSiCl agreed well with the experimental spectra.

The equilibrium geometries and vibrational constants of NO_2^- and NO_2 have been studied by some experimental[1,15–20] and theoretical works.[21–25] These molecules show characteristic geometrical changes between NO_2^- and NO_2 and the adiabatic electron affinity of NO_2 has also been investigated experimentally[1,18,26,27] and theoretically.[28]

In the present article, we apply the direct SAC-CI method[29] and its analytical energy gradient method[11–13] to the X^1A_1 state of NO_2^- and the X^2A_1 state of NO_2 for calculating the equilibrium geometries, vibrational frequencies, and adiabatic electron affinities. The vibrational harmonic frequencies were calculated numerically from the analytical first derivatives and the anharmonicities were evaluated from the 3-dimensional (3D) PESs around the local minima. The vibrational and rotational structures in the photoelectron spectra of NO_2^- was extensively investigated with the SAC-CI theory and compared with the fine experimental spectra observed by Ervin et al.[1] The geometrical change between NO_2^- and NO_2 could be qualitatively interpreted based on the electrostatic force (ESF) theory.[30,31]

Computational Details

The geometry optimizations of NO_2^- and NO_2 were performed with the analytical energy gradients methods of the SAC and SAC-CI, respectively. The vibrational harmonic frequencies were obtained from the second derivatives numerically calculated from the analytical first derivatives. All SAC/SAC-CI calculations were done without perturbation selections. The 1s core orbitals were treated as frozen orbitals and all other orbitals were chosen as

T. Miyahara, H. Nakatsuji
Quantum Chemistry Research Institute, Kyoto Technoscience Center 16, 14 Yoshida Kawara-machi, Sakyou-ku, Kyoto 606-8305, Japan
E-mail: h.nakatsuji@qcri.or.jp

This article is dedicated to the Late Professor Keiji Morokuma for his enormous achievements not only in chemical sciences, in particular in the studies of chemical reactions and homogeneous catalyses, but also in the educational and humanitarian activities as a leader of his scientific group and of the world-wide scientific associations and academies.

Contract Grant sponsor: JSPS; Contract Grant numbers: 17H06233, 16H02257, 15K05408

active orbitals. To find the basis set that gives a reasonable result with low computational cost, the basis set dependences of the equilibrium geometries and the adiabatic electron affinity were examined with 10 basis sets of Dunning's correlation-consistent polarized cc-pVTZ level[32]: (1) cc-pVTZ(−f), (2) cc-pVTZ(−f) + anion p function,[33] (3) cc-pVTZ(−f) + anion p function + Rydberg spd functions,[33] (4) cc-pVTZ(−f) + anion spd function, (5) cc-pVTZ (−f) + anion spd function + Rydberg spd functions, (6) aug-cc-pVTZ(−f),[34] (7) cc-pVTZ, (8) cc-pVTZ + anion p function, (9) cc-pVTZ + anion spd function, (10) aug-cc-pVTZ, where -f indicates that the f-type polarization functions were removed. Then, we used the set, (10) aug-cc-pVTZ, in the following calculations.

For evaluating anharmonic vibrational frequencies, 3-dimensinal potential energy surfaces (3D PESs) were calculated around the local minima with 3375 and 1521 geometric points (15 × 15 × 15 and 13 × 13 × 9 points) for NO_2^- and NO_2, respectively, to cover the regions of the 3D vibrational wavefunctions. As seen in Figure 1, the 3D PESs are shallow for NO_2^- but deep for NO_2, so that different numbers of grid points were used. The 3D PESs were described in the binding coordinates (r_1, r_2, θ) where r_1 and r_2 are the bond distances and θ defines the bond angle. For calculating the vibrational wave functions, these energy points were fitted with the 3D sixth-order Morse–Cosine function,

$$V(r_1,r_2,\theta)=\sum_{i,j,k=0}^{6} B_{ijk}\left(1-e^{-a_1\left(r_1-r_{e_1}\right)}\right)^i \left(\cos\theta-\cos\theta_e\right)^j\left(1-e^{-a_2\left(r_2-r_{e_2}\right)}\right)^k, \quad (1)$$

where r_{e_1}, r_{e_2}, and θ_e are the equilibrium values. The linear parameters $\{B_{ijk}\}$ were obtained with a least-square fitting by varying the nonlinear parameters (a_1, a_2). The fitting of the 3D-PES was satisfactory: the mean deviations from the *ab initio* values at 3375 and 1521 geometric points were less than 0.5 and 0.2 cm^{-1} for NO_2^- and NO_2, respectively. The results guarantee the accuracy of the vibrational energy levels and the wavefunctions including anharmonicity.

For simulating the vibrational spectrum, 3D vibrational states were calculated by the grid method, in which the Lanczos algorithm was used for the diagonalization. In the binding coordinates, the kinetic part of the Hamiltonian (J = 0) of the vibrational motion of A-B-C system is given by,[35,36]

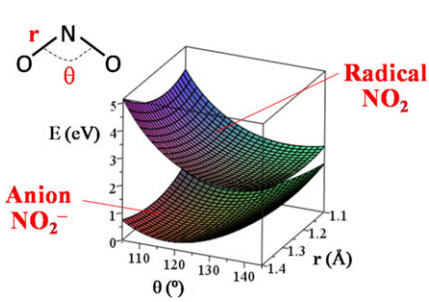

Figure 1. Potential energy surfaces of NO_2^- and NO_2. [Color figure can be viewed at wileyonlinelibrary.com]

$$T=\frac{p_1^2}{2\mu_{AB}}+\frac{p_2^2}{2\mu_{BC}}+\frac{j^2}{2\mu_{AB}r_1^2}+\frac{j^2}{2\mu_{BC}r_2^2}+\frac{p_1p_2\cos\theta}{m_B} -\frac{p_1p_\theta}{m_Br_2}-\frac{p_2p_\theta}{m_Br_1}-\frac{\cos\theta j^2+j^2\cos\theta}{2m_Br_1r_2}, \quad (2)$$

where.

$$p_k=-i\frac{\partial}{\partial r_k}, k=1,2,\ p_\theta=-i\frac{\partial}{\partial\theta}\sin\theta,\ j^2=-\frac{1}{\sin\theta}\frac{\partial}{\partial\theta}\sin\theta\frac{\partial}{\partial\theta} \quad (3)$$

and μ_{AB} and μ_{BC} are the reduced mass of the A–B and B–C systems, respectively. The coordinates r_1 and r_2 are represented by the Hermite discrete variable representation (DVR) with 30 points and θ by the Legendre DVR of 60 points. Thus, the 3D vibrational wavefunction is represented as the grid points,[37]

$$x_j(x)=\left(2^jj!\right)^{-1/2}(m\omega/\pi)^{1/4}H_j\left(\sqrt{m\omega}(x-\tilde{x})\right)e^{-m\omega\left(x-\tilde{x}\right)^2/2}, \quad (4)$$

where H_j denotes the jth Hermite polynomial and x, $\tilde{x}$, ω, and m are the position, the equilibrium position, the frequency and the mass, respectively, and

$$\chi_{l-m+1}(\theta)=\sqrt{\frac{2l+1}{2}\frac{(l-m)!}{(l+m)!}}P_l^m\cos(\theta), \quad (5)$$

where

$$P_l^m(x)=\frac{(-1)^m}{2^ll!}\left(1-x^2\right)^{m/2}\frac{d^{l+m}}{dx^{l+m}}\left(x^2-1\right)^l. \quad (6)$$

The Franck–Condon (FC) factors were calculated with the 3D vibrational wavefunctions.

For calculating the rotational effects, we treated the NO_2 molecule approximately as a symmetric top molecule (A > B = C) whose rotational energy levels are given by

$$E_{JK}=BJ(J+1)+(A-B)K^2,\ |K|\le J,\ \Delta J=0,\pm1 \quad (7)$$

where J and K are quantum numbers for total rotational angular momentum and for the projection of J onto the principal z axis of the molecule, respectively. For the rotational constants A, B, and C, 7.7219, 0.4417, and 0.4178 cm^{-1} obtained from the SAC-CI calculations with the aug-cc-pVTZ basis set for NO_2 were used. The relative intensity of each rotational energy level is obtained by

$$I_{JK}=\exp\left(-\frac{hc}{kT}E_{JK}\right), \quad (8)$$

where h, c, k, and T represent the Planck constant, speed of light, Boltzmann constant and absolute temperature, respectively. In this article, both J and K were considered up to 10.

The SAC/SAC-CI calculations were performed using the development version of the Gaussian09 suite of programs.[38] The vibrational wavefunctions were calculated using the MCTDH program package by Worth et al.[37] Gaussian functions are used as initial functions,

$$\phi(x) = Ne^{-1/4((x-x_0)/\Delta x)^2} e^{ip_0(x-x_0)}, \quad (9)$$

where N is a normalization constant, x_0 and p_0 are the center and initial momentum, and Δx is the width.

Geometries and Adiabatic Electron Affinity

In Tables 1 and 2, we summarized the SAC/SAC-CI results of the geometrical parameters of NO_2^- and NO_2, and the adiabatic electron affinity of NO_2 calculated with several different basis sets. These results are compared with the experimental values[1,15–18,26,27] and the previous theoretical results.[21–25,28]

First, we examine the results shown in Table 1. For NO_2, the geometric parameters obtained by the nonvariational SAC-CI calculations are r_{NO} = 1.1905 Å, and θ_{ONO} = 133.134° with aug-cc-pVTZ basis in good agreement with the experimental values of r_{NO} = 1.19389 Å and θ_{ONO} = 133.514°. The r_{NO} length is longer with the cc-pVTZ(−f) series and shorter with the cc-pVTZ series than the experimental value, but the basis set dependence is very small. However, for θ_{ONO}, the calculated values reduce and depart from the experimental value with the improvement of basis sets. For θ_{ONO}, the SAC-CI values tend to be smaller than the previous theoretical results.

For NO_2^-, the SAC results r_{NO} = 1.2456 Å and θ_{ONO} = 117.114° with aug-cc-pVTZ are in good agreement with the experimental values r_{NO} = 1.25 Å and θ_{ONO} = 117.5°. The basis set dependence is slightly larger than that of NO_2, because the diffuse or anion functions are important for the anion (NO_2^-). The r_{NO} is reduced by the basis set improvement like NO_2. However, the θ_{ONO} of NO_2^- is enlarged by the basis set improvement and its SAC values are larger than the previous theoretical results. This trend is opposite to that of NO_2.

Next, we investigate the electron affinity of NO_2 shown in Table 2. The adiabatic electron affinity with the aug-cc-pVTZ basis sets is calculated to be 2.114 eV in good agreement with the experimental value of 2.273 eV, although the electron affinity is difficult quantity. The adiabatic electron affinity comes close to the experimental value by 0.628 eV by the basis set improvement. The 0–0 band value (2.137 eV with the aug-cc-pVTZ basis set) is slightly closer to the experimental value, because the potential energy surface is shaper for NO_2 than for NO_2^- as shown in Figure 1. To reproduce the adiabatic electron affinity, the diffuse or anion functions are important and necessary.

Thus, the diffuse and anion functions are important for the calculations of the geometrical parameters and electron affinity. Therefore, the aug-cc-pVTZ basis sets were used for the calculations of the photoelectron spectra of NO_2^-.

Vibrational Frequencies

We now start fine theoretical analyses of the photoelectron spectra of NO_2^- observed by Ervin et al.[1] We first examine the vibrational structures of the spectrum observed at 350 K. To

Table 1. Optimized geometries of NO_2^- and NO_2 using the SAC/SAC-CI method.

	Anion [NO_2^-]		Radical [NO_2]	
Basis set	r_{NO}(Å)	θ_{ONO}(°)	r_{NO}(Å)	θ_{ONO}(°)
cc-pVTZ(−f)	1.2598	116.074	1.1955	133.668
cc-pVTZ(−f) + anion (p)	1.2608	115.902	1.1957	133.617
cc-pVTZ(−f) + anion (p) + Rydberg(s,p,d)	1.2571	116.597	1.1963	133.367
cc-pVTZ(−f) + anion(s,p,d)	1.2574	116.562	1.1963	133.404
cc-pVTZ(−f) + anion (s,p,d) + Rydberg(s,p,d)	1.2570	116.585	1.1963	133.335
aug-cc-pVTZ(−f)	1.2551	116.730	1.1959	133.213
cc-pVTZ	1.2501	116.440	1.1893	133.952
cc-pVTZ + anion(p)	1.2505	116.293	1.1893	134.034
cc-pVTZ + anion(s,p,d)	1.2471	116.994	1.1903	133.640
aug-cc-pVTZ	1.2456	117.114	1.1905	133.134
Exptl. (microwave) [a]			1.1934	134.4
Exptl. (infrared, microwave) [b]			1.19455	133.851
Exptl. (microwave) [c]			1.19389	133.514
Exptl. (photoelectron spectroscopy) [d]	1.25	117.5		
Exptl. (photodetachment threshold 1) [e]	1.15	119.5		
Exptl. (photodetachment threshold 2) [e]	1.25	116		
B3LYP/6–311 + G (2d,2p) [f]	1.2584	116.749	1.1940	134.327
CCSD(T)/6–311 + G(2d,p) [f]	1.2725	115.834	1.2041	134.081
SCF [g]	1.265	118	1.212	134
MC-SCF(OVC-CI) [h]			1.199	134.5
MRSDCI [i]			1.185	135
CASSCF [j]	1.260	116.5		

[a] Reference.[15]
[b] Reference.[16]
[c] Reference.[17]
[d] Reference.[1]
[e] Reference.[18]
[f] Reference.[21]
[g] Reference.[22]
[h] Reference.[23]
[i] Reference.[24]
[j] Reference.[25]

Table 2. Adiabatic electron affinity of NO_2 using the SAC/SAC-CI method.

Basis set	Adiabatic electron affinity (0–0 band) (eV)
cc-pVTZ(−f)	1.486
cc-pVTZ(−f) + anion (p)	1.843
cc-pVTZ(−f) + anion (p) + Rydberg(s,p,d)	2.005
cc-pVTZ(−f) + anion(s,p,d)	2.020
cc-pVTZ(−f) + anion (s,p,d) + Rydberg(s,p,d)	2.022
aug-cc-pVTZ(−f)	2.051
cc-pVTZ	1.519
cc-pVTZ + anion(p)	1.866
cc-pVTZ + anion(s,p,d)	2.047
aug-cc-pVTZ	2.114 (2.137)[a]
Exptl.(laser photoelectron spectroscopy)[b]	2.273
Exptl. (laser photodetachment) [c]	2.275
Exptl. (ion/molecule reaction equilibrium)[d]	2.30
Exptl. (electron capture detector)[e]	2.11
B3LYP/aug-cc-pVTZ [f]	2.248
CCSD(T)/aug-cc-pVDZ [f]	2.188

[a] 0–0 band in parentheses.
[b] Reference.[1]
[c] Reference.[18]
[d] Reference.[26]
[e] Reference.[27]
[f] Reference.[28]

investigate the vibrational structures in the observed spectra, the first necessary information is the harmonic and anharmonic vibrational frequencies of NO_2^- and NO_2. Among them, the frequencies of NO_2 are of particular importance.

The vibrational harmonic (ω_1, ω_2, ω_3) and anharmonic (ν_1, ν_2, ν_3) frequencies of NO_2^- and NO_2 have also been calculated with the SAC/SAC-CI method and are summarized in Table 3 together with other theoretical[21,23–25] and experimental values.[1,19,20] The experimental values are fundamental vibrational frequencies, and therefore, theoretical vibrational frequencies including anharmonicity can be compared. However, for the SAC/SAC-CI results, the vibrational anharmonic frequencies are larger than the experimental values. The ν_2 vibrational frequency in NO_2 is smaller than that in NO_2^-, because the atomic dipole (AD) force decreases in NO_2.[30,31] However, the ν_1 and ν_3 vibrational frequency in NO_2 is larger than those in NO_2^- due to the electron removal from the bonding orbital of NO_2^-. Since the deviation of the vibrational anharmonic frequencies from the experimental values was 79, 25, 72 cm^{-1} (0.0098, 0.0031, 0.0089 eV) for υ_1, υ_2, υ_3 of NO_2, the peak positions of the SAC-CI photoelectron spectra are deviated from the experimental ones. For example, the deviation (Δ) of $1_0^n 2_0^m 3_0^l$ from the experimental value is approximately estimated by the following equation,

$$\Delta = 0.0098 \times n + 0.0031 \times m + 0.0089 \times l. \quad (10)$$

Therefore, the deviation becomes large in the lower electron kinetic energy region.

Photoelectron Spectra of NO_2^-

The photoelectron spectra of NO_2^- were observed by the photodetachment of NO_2^-.[1] We calculated the 3D PESs of NO_2^- and NO_2 and evaluated the Franck–Condon factors between NO_2^- and NO_2 using aug-cc-pVTZ basis sets from the vibrational wavefunctions obtained by the MCTDH calculations. The calculated SAC-CI photoelectron spectra of NO_2^- at 350 K and 700 K are compared with the experimental ones in Figures 2 and 3, respectively. In Figure 4, the spectral shape with the rotational effect at 350 K and 700 K is compared with that without the rotational effect. The SAC-CI spectra with the rotational effects at 350 K and 700 K are shown in Figures 5 and 6, respectively. In the SAC-CI spectra, the electron kinetic energies of the vibrational states are shifted by 0.136 eV (= 2.273 (experimental binding energy) – 2.137 (0–0 band energy of SAC/SAC-CI), shown in Table 2) to fit the 0–0 transition at 350 K. The

Table 3. Harmonic and anharmonic vibrational frequencies (cm^{-1}) of NO_2^- and NO_2.

	Method	ω_1	ω_2	ω_3	ν_1	ν_2	ν_3
NO_2^-	SAC	1401	820	1390	1367	811	1335
	B3LYP/6–311 + G (2d,2p) [b]	1327	794	1283			
	QCISD(T)/6-311G(2d,p) [b]	1303	776	1256			
	CASSCF [c]	1316	795	1270	1286	782	1232
	exptl. [d,e]				1284 [d]	776 [d]	1244 [e]
	Δ[f]				83	35	91
NO_2	SAC-CI	1421	787	1731	1397	775	1690
	B3LYP/6–311 + G (2d,2p) [b]	1381	761	1672			
	QCISD(T)/6-311G(2d,p) [b]	1315	748	1602			
	MC-SCF(OVC-CI) [g]	1351	758				
	MRSDCI [h]	1500	793				
	exptl. [i]				1318	750	1618
	Δ[f]				79	25	72

ω_1, ν_1: symmetric-stretching mode, ω_2,ν_2: bending mode, ω_3, ν_3: asymmetric-stretching mode.
[b] Reference.[21]
[c] Reference.[25]
[d] Reference.[1]
[e] Reference.[19]
[f] [SAC-CI] – [exptl.].
[g] Reference.[23]
[h] Reference.[24]
[i] Reference.[20]

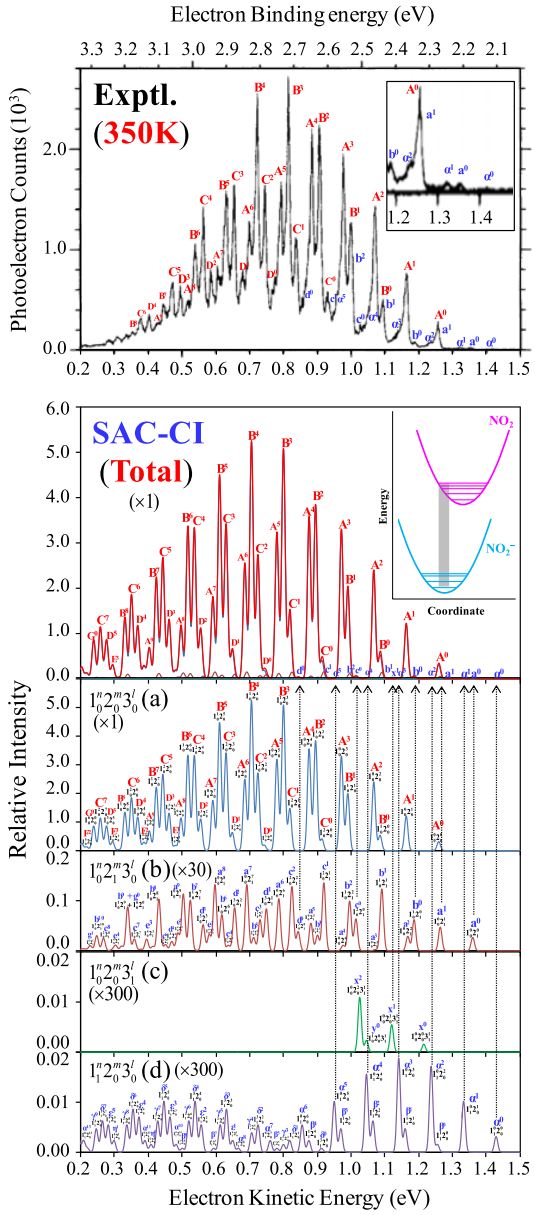

Figure 2. Experimental and SAC-CI photoelectron spectra of NO_2^- at 350 K. The SAC-CI theoretical spectrum (total) is the sum of the contributions from the vibrational ground state ($1_02_03_0$(a)) and from the vibrational excited states ($1_02_13_0$(b), $1_02_03_1$(c), and $1_12_03_0$(d)). The inset of the experimental spectrum shows the enlarged view of the range 1.2 eV–1.5 eV in the electron kinetic energy. The inset of the SAC-CI spectrum (Total) shows the schematic diagram of the vibrational excitations accompanying to the ionization from NO_2^- to NO_2. Horizontal axis represents the vibrational coordinate. [Color figure can be viewed at wileyonlinelibrary.com]

SAC-CI spectra at 700 K are shifted by 0.141 eV due to the deviation (0.005 eV) in the experimental spectra between at 350 K and 700 K. The full width at half-maximum of the Gaussian envelope was 0.012 eV for the SAC-CI photoelectron spectra in Figures 2 and 5, but 0.008 eV in Figures 3,4, and 6. The horizontal axis scale is electron binding energy for the upper side and the electron kinetic energy for the lower side in Figures. The scale on the vertical axis of the SAC-CI results shows relative intensity. The detailed vibrational assignments of all the peaks at 300 K and 700 K are summarized in Tables 4 and 5, respectively, with the electron kinetic energy in accordance with the experimental condition.[1] The assignments of the peaks in the higher electron kinetic energy region at 700 K are summarized in Table 6. These Figures and Tables are important data for analyzing and understanding the experimental photoelectron spectra. In Figures and Tables, the labels A^n, B^n, C^n, D^n, E^n, F^n, and G^n represent the vibrational levels $1_0^02_0^n3_0^0$, $1_0^12_0^n3_0^0$,

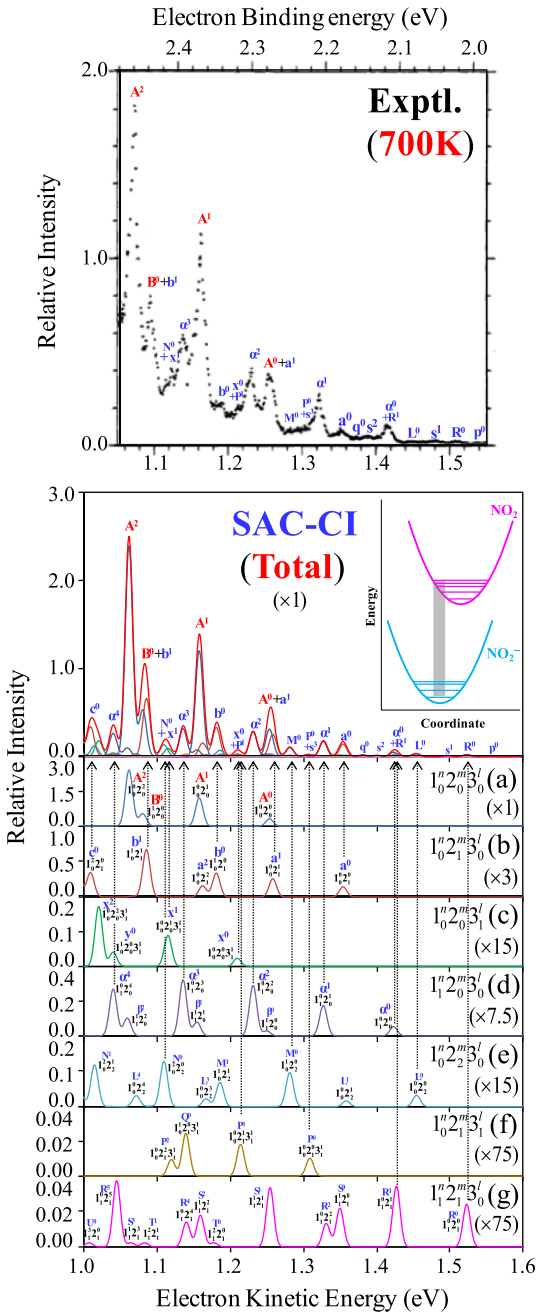

Figure 3. Experimental and SAC-CI photoelectron spectra of NO_2^- at 700 K. The SAC-CI theoretical spectrum (total) is the sum of the contributions from the vibrational ground state ($1_02_03_0$(a)) and from the vibrational excited states ($1_02_13_0$(b), $1_02_03_1$(c), $1_12_03_0$(d), $1_02_23_0$(e), $1_02_13_1$(f), and $1_12_13_0$(g)). The inset of the SAC-CI spectrum (Total) shows the schematic diagram of the vibrational excitations accompanying to the ionization from NO_2^- to NO_2. Horizontal axis represents the vibrational coordinate. [Color figure can be viewed at wileyonlinelibrary.com]

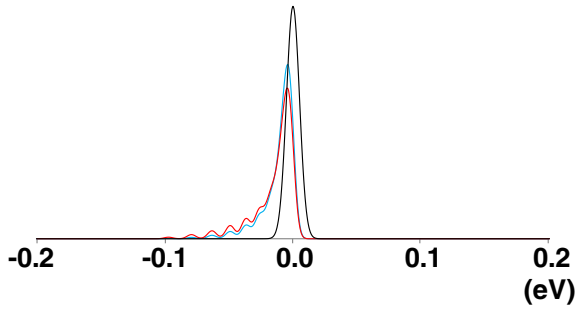

Figure 4. Spectral shapes with the rotational effects at 350 K (blue line) and 700 K (red line) are compared with that (black line) without the rotational effects. [Color figure can be viewed at wileyonlinelibrary.com]

$1_0^2 2_0^n 3_0^0$, $1_0^3 2_0^n 3_0^0$, $1_0^4 2_0^n 3_0^0$, $1_0^5 2_0^n 3_0^0$, and $1_0^6 2_0^n 3_0^0$, respectively, where 1, 2, and 3 denote υ_1, υ_2, and υ_3, respectively, and the subscript and superscript represent the vibrational levels of NO_2^- and NO_2, respectively. The labels a^n, b^n, c^n, d^n, e^n, f^n, and g^n represent the vibrational levels $1_0^0 2_1^n 3_0^0$, $1_0^1 2_1^n 3_0^0$, $1_0^2 2_1^n 3_0^0$, $1_0^3 2_1^n 3_0^0$, $1_0^4 2_1^n 3_0^0$, $1_0^5 2_1^n 3_0^0$, and $1_0^6 2_1^n 3_0^0$, respectively. The labels x^n and y^n represent the vibrational levels $1_0^0 2_0^n 3_1^1$ and $1_0^1 2_0^n 3_1^1$, respectively. The labels α^n, β^n, γ^n, δ^n, ε^n, ζ^n, and η^n represent the vibrational levels $1_1^0 2_0^n 3_0^0$, $1_1^1 2_0^n 3_0^0$, $1_1^2 2_0^n 3_0^0$, $1_1^3 2_0^n 3_0^0$, $1_1^4 2_0^n 3_0^0$, $1_1^5 2_0^n 3_0^0$, and $1_1^6 2_0^n 3_0^0$, respectively. The vibrational mode 3_0^0 is omitted in Figures, Tables and the following text. The labels L^n, M^n, N^n, P^n, Q^n, R^n, S^n, T^n, and U^n represent the vibrational levels $1_0^0 2_2^n 3_0^0$, $1_0^1 2_2^n 3_0^0$, $1_0^2 2_2^n 3_0^0$, $1_0^0 2_1^n 3_1^1$, $1_0^1 2_1^n 3_1^1$, $1_0^0 2_1^n 3_0^0$, $1_1^1 2_1^n 3_0^0$, $1_1^2 2_1^n 3_0^0$, and $1_1^3 2_1^n 3_0^0$, respectively. The labels p^n, q^n, r^n, s^n, u^n, v^n, and w^n represent the vibrational levels $1_0^0 2_3^n 3_0^0$, $1_0^1 2_3^n 3_0^0$, $1_0^0 2_0^n 3_1^1$, $1_0^0 2_0^n 3_0^0$, $1_1^0 2_2^n 3_0^0$, $1_1^1 2_2^n 3_0^0$, and $1_0^2 2_4^n 3_0^0$, respectively. These notations are summarized in Table 7.

In Figure 2, the SAC-CI spectrum at 350 K includes the ionizations not only from the vibrational ground state ($1_0 2_0 3_0$) but also from vibrational excited states ($1_0 2_1 3_0$, $1_0 2_0 3_1$, and $1_1 2_0 3_0$). The schematic diagram of the vibrational excitations accompanying to the ionization from NO_2^- to NO_2 is shown in the inset of the SAC-CI spectrum (Total). The ratios of the $1_0 2_0 3_0$, $1_0 2_1 3_0$, $1_0 2_0 3_1$, and $1_1 2_0 3_0$ are 1, 0.0357, 0.0041, and 0.0036 with respect to the $1_0 2_0 3_0$ determined by the Boltzmann distribution at 350 K. The scales in Figures 2b–2d are different from that in Figure 2a, because the intensities of $1_0^n 2_1^m 3_0^l$, $1_0^n 2_0^m 3_1^l$, and $1_1^n 2_0^m 3_0^l$ are much different from that of $1_0^n 2_0^m 3_0^l$. We show in Figure 2a the spectrum from the $1_0 2_0 3_0$ state with the ratio unity, Figure 2b the one from the $1_0 2_1 3_0$ state with the ratio 30, Figure 2c the one from the $1_0 2_0 3_1$ state with the ratio 300, and Figure 2d the one from the $1_1 2_0 3_0$ state with the ratio 300. The SAC-CI spectrum (Total) of Figure 2 is the sum of the contributions as expressed by

$$\text{Fig.2(total)} = \text{Fig.2(a)} + \frac{1}{30}\text{Fig.2(b)} + \frac{1}{300}\text{Fig.2(c)} + \frac{1}{300}\text{Fig.2(d)}. \quad (11)$$

In Figure 3, the SAC-CI spectrum at 700 K includes further the ionizations from higher vibrational excited states ($1_0 2_2 3_0$, $1_0 2_1 3_1$, and $1_1 2_1 3_0$). The ratios of the $1_0 2_0 3_0$, $1_0 2_1 3_0$, $1_0 2_0 3_1$, $1_1 2_0 3_0$, $1_0 2_2 3_0$, $1_0 2_1 3_1$, and $1_1 2_1 3_0$ with respect to the $1_0 2_0 3_0$ at 700 K are 1, 0.1889, 0.0643, 0.0601, 0.0358, 0.0124, and 0.0115. The scales in Figures 3b–3g are different from that in Figure 3a, because the intensities of $1_0^n 2_1^m 3_0^l$, $1_0^n 2_0^m 3_1^l$, $1_1^n 2_0^m 3_0^l$, $1_0^n 2_2^m 3_0^l$, $1_0^n 2_1^m 3_1^l$, and $1_1^n 2_1^m 3_0^l$ are much different from that of $1_0^n 2_0^m 3_0^l$. We show in Figure 3a the spectrum from the $1_0 2_0 3_0$ state with the ratio unity, Figure 3b the one from the $1_0 2_1 3_0$ state with the ratio 3, Figure 3c the one from the $1_0 2_0 3_1$ state with the ratio 15, Figure 3d the one from the $1_1 2_0 3_0$ state with the ratio 7.5,

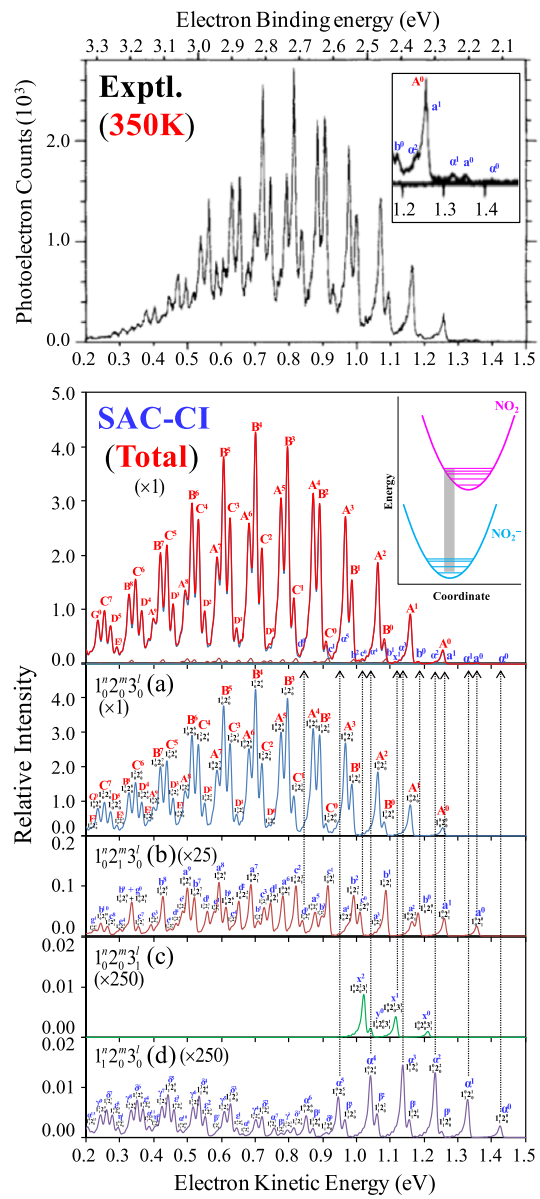

Figure 5. Experimental and SAC-CI photoelectron spectra of NO_2^- at 350 K including rotational effects. The SAC-CI theoretical spectrum (total) is the sum of the contributions from the vibrational ground state ($1_0 2_0 3_0$(a)) and from the vibrational excited states ($1_0 2_1 3_0$(b), $1_0 2_0 3_1$(c), and $1_1 2_0 3_0$(d)). The inset of the experimental spectrum shows the enlarged view of the range 1.2 eV–1.5 eV in the electron kinetic energy. The inset of the SAC-CI spectrum (Total) shows the schematic diagram of the vibrational excitations accompanying to the ionization from NO_2^- to NO_2. Horizontal axis represents the vibrational coordinate. [Color figure can be viewed at wileyonlinelibrary.com]

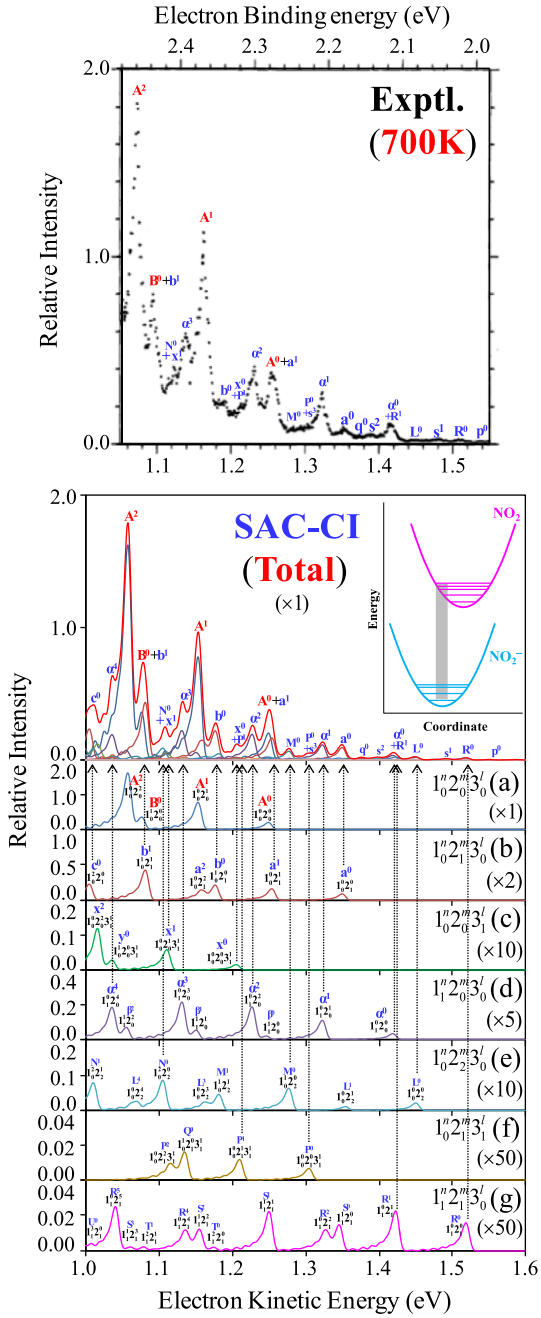

Figure 6. Experimental and SAC-CI photoelectron spectra of NO_2^- at 700 K including rotational effects. The SAC-CI theoretical spectrum (total) is the sum of the contributions from the vibrational ground state ($1_0 2_0 3_0$(a)) and from the vibrational excited states ($1_0 2_1 3_0$(b), $1_0 2_0 3_1$(c), $1_1 2_0 3_0$(d), $1_0 2_2 3_0$(e), $1_0 2_1 3_1$(f), and $1_1 2_1 3_0$(g)). The inset of the SAC-CI spectrum (Total) shows the schematic diagram of the vibrational excitations accompanying to the ionization from NO_2^- to NO_2. Horizontal axis represents the vibrational coordinate. [Color figure can be viewed at wileyonlinelibrary.com]

Figure 3e the one from the $1_0 2_2 3_0$ state with the ratio 15, Figure 3f the one from the $1_0 2_1 3_1$ state with the ratio 75, and Figure 3g the one from the $1_1 2_1 3_0$ state with the ratio 75. The total SAC-CI spectrum includes further the ionizations from 7th to 13th vibrational excited states with the ratios of 0.0068, 0.0043, 0.0040, 0.0036, 0.0024, 0.0022, and 0.0013, respectively. These ionizations are shown not in the Figure but in Tables 5 and 6. The SAC-CI spectrum (Total) of Figure 3 is the sum of the contributions as expressed by

$$\text{Fig.3(total)} = \text{Fig.3(a)} + \frac{1}{3}\text{Fig.3(b)} + \frac{1}{15}\text{Fig.3(c)} + \frac{1}{7.5}\text{Fig.3(d)} + \frac{1}{15}\text{Fig.3(e)} + \frac{1}{75}\text{Fig.3(f)} + \frac{1}{75}\text{Fig.3(g)}. \quad (12)$$

Photoelectron Spectrum at 350 K

Referring to Figure 2, we see that the experimental spectrum at 350 K almost comes from the ionization from the vibrational ground state ($1_0 2_0 3_0$). The contributions of the ionizations from other states are less than 4.5% in total. Therefore, in Figure 2, the total SAC-CI spectrum is almost the same as the spectrum denoted as $1_0^n 2_0^m 3_0^l$(a). The SAC-CI spectra are in good agreement with the experimental spectra in the high electron kinetic energy region. However, since the theoretical vibrational anharmonic frequencies of NO_2 (υ_1, υ_2, υ_3) are larger than the experimental values, the deviation between the SAC-CI and the experimental spectra becomes larger as the electron kinetic energy becomes lower as shown in Table 4.

The experimental peak at 1.259 eV is assigned to the theoretical peak A^0 ($1_0^0 2_0^0$) of the 0–0 transition that is the ionization from the vibrational ground states of the ground state (X^1A_1) of NO_2^- to the vibrational excited states of the ground state (X^2A_1) of NO_2. The shoulder peak is observed in the right-hand side (higher electron kinetic energy region) of the peak A^0, because the peak a^1(b) (b in parentheses means Fig. 2b) with some intensity is calculated to be in the right side of the peak A^0. The nature of the peak a^1 is the $1_0^0 2_1^1$, which is the ionization from the bending vibrational excited state of NO_2^- to the bending vibrational excited state of NO_2.

There are three peaks with a very small intensity in the range of 1.3–1.5 eV electron kinetic energy of the experimental spectrum. The enlarged view is shown in the inset of the experimental spectrum in Figure 2. The experimental peaks at 1.420 eV, 1.353 eV, and 1.321 eV are assigned to the theoretical peaks α^0(d), a^0(b), and α^1(d), respectively. The a^n ($1_0^0 2_1^n 3_0^0$) and α^n ($1_1^0 2_0^n 3_0^0$) are the ionizations from the bending and symmetric-stretching vibrational excited states of NO_2^-, respectively. The ionizations from the vibrational excited states are observed in the higher electron kinetic energy region than the 0–0 transition.

There are two small peaks between two strong peaks (A^0 and A^1) in the experiment. The experimental peaks at 1.237 eV and 1.187 eV are assigned to the peaks α^2(d) and b^0(b), respectively. The peak α^2 ($1_1^0 2_0^2$) is the ionization to the first overtone bending mode of NO_2. The peak b^0 ($1_0^1 2_1^0$) is the ionization from the bending mode of NO_2^- to the symmetric-stretching mode of NO_2. The peak x^0(c) with a very small intensity is calculated to be between two peaks α^2 and b^0. The nature of the peak x^0 is the $1_0^0 2_0^0 3_1^1$, which is the ionization between the asymmetric-stretching modes of NO_2^- and NO_2. Therefore, the experimental spectrum may be broad between the peaks α^2 and b^0.

Table 4. Vibrational levels, electron kinetic energy, Franck–Condon factor (FCF) of the photoelectron spectrum of NO_2^- at 350 K by the SAC-CI 3-dimensional potential energy surfaces (3D PESs).

Assignment of peak [a]	Exptl. electron kinetic energy (eV)	SAC-CI State	SAC-CI electron kinetic energy (eV)	SAC-CI FCF
α^0	1.420	$1^0_1 2^0_0$	1.429	0.00004
a^0	1.353	$1^0_0 2^0_1$	1.360	0.00034
α^1	1.321	$1^0_1 2^1_0$	1.333	0.00013
a^1		$1^0_0 2^1_1$	1.264	0.00061
A^0	1.259	$1^0_0 2^0_0$	1.259	0.00401
β^0		$1^1_1 2^0_0$	1.255	0.00002
α^2	1.237	$1^0_1 2^2_0$	1.237	0.00022
x^0	1.210	$1^0_0 2^0_0 3^1_1$	1.215	0.00002
b^0	1.187	$1^1_0 2^0_1$	1.186	0.00080
a^2		$1^0_0 2^2_1$	1.168	0.00037
A^1	1.162	$1^0_0 2^1_0$	1.163	0.01538
β^1		$1^1_1 2^1_0$	1.160	0.00006
α^3	1.135	$1^0_1 2^3_0$	1.141	0.00024
x^1	1.115	$1^0_0 2^1_0 3^1_1$	1.120	0.00007
b^1		$1^1_0 2^1_1$	1.091	0.00159
B^0	1.093	$1^1_0 2^0_0$	1.086	0.00678
a^3		$1^0_0 2^3_1$	1.072	0.00003
A^2	1.070	$1^0_0 2^2_0$	1.067	0.03057
β^2		$1^1_1 2^2_0$	1.065	0.00008
α^4		$1^0_1 2^4_0$	1.046	0.00020
y^0		$1^1_0 2^0_0 3^1_1$	1.045	0.00003
x^2		$1^0_0 2^2_0 3^1_1$	1.026	0.00014
c^0	1.027	$1^2_0 2^0_1$	1.014	0.00082
b^2		$1^1_0 2^2_1$	0.996	0.00128
B^1	1.000	$1^1_0 2^1_0$	0.990	0.02538
a^4		$1^0_0 2^4_1$	0.977	0.00014
A^3	0.977	$1^0_0 2^3_0$	0.971	0.04209
β^3		$1^1_1 2^3_0$	0.970	0.00006
α^5		$1^0_1 2^5_0$	0.950	0.00013
c^1		$1^2_0 2^1_1$	0.920	0.00175
C^0	0.930	$1^2_0 2^0_0$	0.914	0.00517
δ^0		$1^3_1 2^0_0$	0.913	0.00001
b^3		$1^1_0 2^3_1$	0.901	0.00040
B^2	0.905	$1^1_0 2^2_0$	0.895	0.04888
a^5		$1^0_0 2^5_1$	0.881	0.00071
A^4	0.883	$1^0_0 2^4_0$	0.876	0.04524
β^4		$1^1_1 2^4_0$	0.875	0.00003
α^6		$1^0_1 2^6_0$	0.856	0.00007
d^0	0.855	$1^3_0 2^0_1$	0.844	0.00049
c^2		$1^2_0 2^2_1$	0.825	0.00165
C^1	0.836	$1^2_0 2^1_0$	0.819	0.01868
δ^1		$1^3_1 2^1_0$	0.819	0.00003
B^3	0.812	$1^1_0 2^3_0$	0.800	0.06481
γ^3		$1^2_1 2^3_0$	0.800	0.00002
a^6		$1^0_0 2^6_1$	0.787	0.00134
β^5		$1^1_1 2^5_0$	0.781	0.00001
A^5	0.792	$1^0_0 2^5_0$	0.781	0.04058
α^7	0.774	$1^0_1 2^7_0$	0.761	0.00003
d^1		$1^3_0 2^1_1$	0.750	0.00108
D^0	0.765	$1^3_0 2^0_0$	0.743	0.00232
c^3		$1^2_0 2^3_1$	0.731	0.00080
δ^2		$1^3_1 2^2_0$	0.725	0.00007
C^2	0.745	$1^2_0 2^2_0$	0.725	0.03451
b^5		$1^1_0 2^5_1$	0.712	0.00034
γ^4		$1^2_1 2^4_0$	0.706	0.00005

(Continues)

Table 4. Continued

Assignment of peak [a]	Exptl. electron kinetic energy (eV)	SAC-CI State	SAC-CI electron kinetic energy (eV)	SAC-CI FCF
B^4	0.722	$1^1_0 2^4_0$	0.706	0.06673
a^7		$1^0_0 2^7_1$	0.692	0.00170
A^6	0.698	$1^0_0 2^6_0$	0.686	0.03175
α^8		$1^0_1 2^8_0$	0.667	0.00001
d^2		$1^3_0 2^2_1$	0.656	0.00111
ε^1		$1^4_1 2^1_0$	0.650	0.00003
D^1	0.680	$1^3_0 2^1_0$	0.649	0.00802
c^4		$1^2_0 2^4_1$	0.637	0.00014
δ^3		$1^3_1 2^3_0$	0.632	0.00011
C^3	0.653	$1^2_0 2^3_0$	0.631	0.04355
b^6		$1^1_0 2^6_1$	0.618	0.00093
γ^5		$1^2_1 2^5_0$	0.613	0.00007
B^5	0.630	$1^1_0 2^5_0$	0.612	0.05709
a^8		$1^0_0 2^8_1$	0.598	0.00170
β^7		$1^1_1 2^7_0$	0.594	0.00001
A^7	0.604	$1^0_0 2^7_0$	0.592	0.02234
e^1		$1^4_0 2^1_1$	0.581	0.00042
d^3		$1^3_0 2^3_1$	0.563	0.00067
ε^2		$1^4_1 2^2_0$	0.557	0.00007
D^2	0.584	$1^3_0 2^2_0$	0.556	0.01402
δ^4		$1^3_1 2^4_0$	0.539	0.00013
C^4	0.562	$1^2_0 2^4_0$	0.537	0.04238
b^7		$1^1_0 2^7_1$	0.525	0.00130
γ^6		$1^2_1 2^6_0$	0.521	0.00008
B^6	0.539	$1^1_0 2^6_0$	0.518	0.04241
a^9		$1^0_0 2^9_1$	0.504	0.00146
β^8		$1^1_1 2^8_0$	0.501	0.00001
A^8	0.519	$1^0_0 2^8_0$	0.497	0.01447
e^2		$1^4_0 2^2_1$	0.488	0.00045
α^{10}		$1^0_1 2^{10}_0$	0.483	0.00002
E^1		$1^4_0 2^1_0$	0.481	0.00223
d^4		$1^3_0 2^4_1$	0.470	0.00024
ε^3		$1^4_1 2^3_0$	0.465	0.00009
D^3	0.495	$1^3_0 2^3_0$	0.462	0.01658
c^6		$1^2_0 2^6_1$	0.452	0.00016
δ^5		$1^3_1 2^5_0$	0.447	0.00013
C^5	0.472	$1^2_0 2^5_0$	0.444	0.03397
b^8		$1^1_0 2^8_1$	0.432	0.00133
γ^7		$1^2_1 2^7_0$	0.429	0.00008
B^7	0.444	$1^1_0 2^7_0$	0.425	0.02821
a^{10}		$1^0_0 2^{10}_1$	0.414	0.00011
η^0		$1^6_1 2^0_0$	0.409	0.00002
A^9	0.425	$1^0_0 2^9_0$	0.404	0.00875
e^3		$1^4_0 2^3_1$	0.396	0.00030
α^{11}		$1^0_1 2^{11}_0$	0.391	0.00003
E^2		$1^4_0 2^2_0$	0.388	0.00362
d^5		$1^3_0 2^5_1$	0.378	0.00004
ε^4		$1^4_1 2^4_0$	0.373	0.00009
D^4	0.402	$1^3_0 2^4_0$	0.370	0.01494
c^7		$1^2_0 2^7_1$	0.360	0.00030
δ^6		$1^3_1 2^6_0$	0.356	0.00011
C^6	0.379	$1^2_0 2^6_0$	0.351	0.02355
b^9		$1^1_0 2^9_1$	0.340	0.00065
g^0		$1^6_0 2^0_1$	0.340	0.00048
γ^8		$1^2_1 2^8_0$	0.338	0.00007
B^8	0.352	$1^1_0 2^8_0$	0.332	0.01708
a^{11}		$1^0_0 2^{11}_1$	0.322	0.00012

(Continues)

Table 4. Continued

Assignment of peak [a]	Exptl. electron kinetic energy (eV)	SAC-CI State	SAC-CI electron kinetic energy (eV)	SAC-CI FCF
A^{10}	0.335	$1^0_0 2^{10}_0$	0.314	0.00041
e^4		$1^4_0 2^4_1$	0.304	0.00014
η^1		$1^6_1 2^1_0$	0.300	0.00003
E^3		$1^4_0 2^3_0$	0.295	0.00392
ε^5		$1^4_1 2^5_0$	0.283	0.00007
D^5	0.307	$1^3_0 2^5_0$	0.278	0.01095
c^8		$1^2_0 2^8_1$	0.269	0.00032
δ^7		$1^3_1 2^7_0$	0.265	0.00008
C^7	0.283	$1^2_0 2^7_0$	0.259	0.01451
b^{10}		$1^1_0 2^{10}_1$	0.249	0.00039
γ^9		$1^2_1 2^9_0$	0.247	0.00005
B^9		$1^1_0 2^9_0$	0.240	0.00168
G^0		$1^6_0 2^0_0$	0.240	0.00926
g^1		$1^6_0 2^1_1$	0.231	0.00009
a^{12}		$1^0_0 2^{12}_1$	0.227	0.00005
A^{11}		$1^0_0 2^{11}_0$	0.222	0.00059
η^2		$1^6_1 2^2_0$	0.221	0.00001
F^2		$1^5_0 2^2_0$	0.217	0.00117
e^5		$1^4_0 2^5_1$	0.214	0.00004
α^{13}		$1^0_1 2^{13}_0$	0.209	0.00003
E^4		$1^4_0 2^4_0$	0.204	0.00318
d^7		$1^3_0 2^7_1$	0.196	0.00001
D^6		$1^3_0 2^6_0$	0.186	0.00680

[a] The labels A^n, B^n, C^n, D^n, E^n, F^n, and G^n represent the vibrational levels $1^0_0 2^n_0 3^0_0$, $1^1_0 2^n_0 3^0_0$, $1^2_0 2^n_0 3^0_0$, $1^3_0 2^n_0 3^0_0$, $1^4_0 2^n_0 3^0_0$, $1^5_0 2^n_0 3^0_0$, and $1^6_0 2^n_0 3^0_0$, respectively, where 1, 2, and 3 denote υ_1, υ_2, and υ_3, respectively and the subscript and superscript represent the vibrational levels of NO_2^- and NO_2, respectively. The labels a^n, b^n, c^n, d^n, e^n, f^n, and g^n represent the vibrational levels $1^0_0 2^n_1 3^0_0$, $1^1_0 2^n_1 3^0_0$, $1^2_0 2^n_1 3^0_0$, $1^3_0 2^n_1 3^0_0$, $1^4_0 2^n_1 3^0_0$, $1^5_0 2^n_1 3^0_0$, and $1^6_0 2^n_1 3^0_0$, respectively. The labels x^n and y^n represent the vibrational levels $1^0_0 2^n_0 3^1_1$ and $1^1_0 2^n_0 3^1_1$, respectively. The labels α^n, β^n, γ^n, δ^n, ε^n, ζ^n, and η^n represent the vibrational levels $1^0_1 2^n_0 3^0_0$, $1^1_1 2^n_0 3^0_0$, $1^2_1 2^n_0 3^0_0$, $1^3_1 2^n_0 3^0_0$, $1^4_1 2^n_0 3^0_0$, $1^5_1 2^n_0 3^0_0$, $1^6_1 2^n_0 3^0_0$, respectively. The vibrational mode 3^0_0 is omitted.

The strong experimental peak (1.162 eV) is assigned to the peak A^1 ($1^0_0 2^1_0$) of the excitation to the bending vibrational excited state of NO_2.

The calculated peak a^2(b,$1^0_0 2^2_1$) may be considered to be the shoulder peak of the peak A^1 with the deviation of 0.005 eV. However, the intensity of the peak a^2 is much smaller than the peak A^1 by the two orders of magnitude. Therefore, we think that the peak a^2 is not observed in the experiment. This is different from the relation between the peaks A^0 and a^1. Two states of the peaks α^3(d,$1^0_1 2^3_0$) and x^1(c,$1^0_0 2^1_0 3^1_1$) with a very small intensity is calculated to be in the left-hand side (lower electron kinetic energy region) of the A^1. The x^1($1^0_0 2^1_0 3^1_1$) is the ionization to the combination of bending and asymmetric-stretching modes of NO_2.

For two strong experimental peaks observed in the range of 1.0–1.1 eV, the weaker peak is assigned to the ionization to the symmetric-stretching mode ($1^1_0 2^0_0$(B^0)) and the strongly one is assigned to the first overtone bending mode ($1^0_0 2^2_0$(A^2)). A small peak b^1(b) is calculated with the difference of 0.005 eV from the peak B^0. The peak b^1 ($1^1_0 2^1_1$) is the ionization to the combination of the bending and symmetric-stretching modes. This corresponds to the shoulder peak observed in the right-hand side of the peak B^0 in the experimental one. The relation

Table 5. Vibrational levels, electron kinetic energy, Franck–Condon factor (FCF) of the photoelectron spectrum of NO_2^- at 700 K by the SAC-CI 3-dimensional potential energy surfaces (3D PESs).

Assignment of peak [a]	Exptl. electron kinetic energy (eV)	SAC-CI State	SAC-CI electron kinetic energy (eV)	SAC-CI FCF
R^0	1.510	$1^0_1 2^0_1$	1.523	0.00031
L^0	1.445	$1^0_0 2^0_2$	1.455	0.00041
R^1	1.415	$1^0_1 2^1_1$	1.427	0.00044
α^0	1.415	$1^0_1 2^0_0$	1.424	0.00067
L^1		$1^0_0 2^1_2$	1.359	0.00021
a^0	1.352	$1^0_0 2^0_1$	1.355	0.00182
S^0		$1^1_1 2^0_1$	1.350	0.00028
R^2		$1^0_1 2^2_1$	1.332	0.00017
α^1	1.324	$1^0_1 2^1_0$	1.328	0.00220
P^0	1.295	$1^0_0 2^0_1 3^1_1$	1.309	0.00013
M^0	1.284	$1^1_0 2^0_2$	1.282	0.00123
a^1	1.254	$1^0_0 2^1_1$	1.259	0.00324
S^1		$1^1_1 2^1_1$	1.255	0.00043
A^0	1.254	$1^0_0 2^0_0$	1.254	0.00401
β^0		$1^1_1 2^0_0$	1.250	0.00036
α^2	1.231	$1^0_1 2^2_0$	1.232	0.00366
P^1	1.213	$1^0_0 2^1_1 3^1_1$	1.215	0.00023
x^0	1.213	$1^0_0 2^0_0 3^1_1$	1.210	0.00030
M^1		$1^1_0 2^1_2$	1.186	0.00088
b^0	1.190	$1^1_0 2^1_1$	1.181	0.00423
T^0		$1^2_1 2^0_1$	1.178	0.00003
L^3		$1^0_0 2^3_2$	1.167	0.00028
a^2		$1^0_0 2^2_1$	1.163	0.00198
S^2		$1^1_1 2^2_1$	1.160	0.00023
A^1	1.162	$1^0_0 2^1_0$	1.158	0.01538
β^1		$1^1_1 2^1_0$	1.155	0.00099
Q^0		$1^1_0 2^0_1 3^1_1$	1.140	0.00031
R^4		$1^0_1 2^4_1$	1.140	0.00018
α^3	1.139	$1^0_1 2^3_0$	1.136	0.00407
P^2		$1^0_0 2^2_1 3^1_1$	1.120	0.00012
x^1	1.121	$1^0_0 2^1_0 3^1_1$	1.115	0.00113
N^0	1.121	$1^2_0 2^0_2$	1.110	0.00164
b^1	1.094	$1^1_0 2^1_1$	1.086	0.00842
T^1		$1^2_1 2^1_1$	1.084	0.00003
B^0	1.094	$1^1_0 2^0_0$	1.081	0.00678
L^4		$1^0_0 2^4_2$	1.072	0.00040
a^3		$1^0_0 2^3_1$	1.067	0.00015
S^3		$1^1_1 2^3_1$	1.065	0.00003
A^2	1.072	$1^0_0 2^2_0$	1.062	0.03057
β^2		$1^1_1 2^2_0$	1.060	0.00129
R^5		$1^0_1 2^5_1$	1.045	0.00048
α^4		$1^0_1 2^4_0$	1.041	0.00340
y^0		$1^1_0 2^0_0 3^1_1$	1.041	0.00052
x^2		$1^0_0 2^2_0 3^1_1$	1.021	0.00219
N^1		$1^2_0 2^1_2$	1.015	0.00151
c^0		$1^2_0 2^0_1$	1.009	0.00434
U^0		$1^3_1 2^0_1$	1.008	0.00003
M^3		$1^1_0 2^3_2$	0.996	0.00041
b^2		$1^1_0 2^2_1$	0.991	0.00679
B^1		$1^1_0 2^1_0$	0.985	0.02538

[a] See footnote of Table 4. The labels L^n, M^n, N^n, P^n, Q^n, R^n, S^n, T^n, and U^n represent the vibrational levels $1^0_0 2^n_2 3^0_0$, $1^1_0 2^n_2 3^0_0$, $1^2_0 2^n_2 3^0_0$, $1^0_0 2^n_1 3^1_1$, $1^1_0 2^n_1 3^1_1$, $1^0_1 2^n_1 3^0_0$, $1^1_1 2^n_1 3^0_0$, $1^2_1 2^n_1 3^0_0$, and $1^3_1 2^n_1 3^0_0$, respectively.

Table 6. Vibrational levels, electron kinetic energy, Franck–Condon factor (FCF) in the higher electron kinetic energy region of the photoelectron spectrum of NO_2^- at 700 K by the SAC-CI 3-dimensional potential energy surfaces (3D PESs).

	Exptl.	SAC-CI			
Assignment of peak[a]	electron kinetic energy (eV)	State	Vibrational level of NO_2^-	Electron kinetic energy (eV)	FCF
u^0		$1^0_1 2^0_2$	12th	1.623	0.00007
s^0		$1^0_2 2^0_0$	10th	1.593	0.00006
p^0	1.538	$1^0_0 2^0_3$	7th	1.555	0.00006
R^0	1.510	$1^0_1 2^0_1$	6th	1.523	0.00031
s^1	1.482	$1^0_2 2^1_0$	10th	1.497	0.00016
L^0	1.445	$1^0_0 2^0_2$	4th	1.455	0.00041
v^0		$1^1_1 2^0_2$	12th	1.450	0.00010
R^1	1.415	$1^0_1 2^1_1$	6th	1.427	0.00044
α^0	1.415	$1^0_1 2^0_0$	3rd	1.424	0.00067
s^2	1.388	$1^0_2 2^2_0$	10th	1.401	0.00021
q^0	1.375	$1^1_0 2^0_3$	7th	1.382	0.00023
r^0		$1^0_1 2^0_0 3^1_1$	9th	1.377	0.00005
L^1		$1^0_0 2^1_2$	4th	1.359	0.00021
a^0	1.352	$1^0_0 2^0_1$	1st	1.355	0.00182
v^1		$1^1_1 2^1_2$	12th	1.355	0.00005
S^0		$1^1_1 2^0_1$	6th	1.350	0.00028
u^3		$1^0_1 2^3_2$	12th	1.336	0.00005
R^2		$1^0_1 2^2_1$	6th	1.332	0.00017
α^1	1.324	$1^0_1 2^1_0$	3rd	1.328	0.00220
w^0		$1^2_0 2^0_4$	13th	1.310	0.00006
P^0	1.295	$1^0_0 2^0_1 3^1_1$	5th	1.309	0.00013
s^3	1.295	$1^0_2 2^3_0$	10th	1.305	0.00019
r^1		$1^0_1 2^1_0 3^1_1$	9th	1.283	0.00016
M^0	1.284	$1^1_0 2^0_2$	4th	1.282	0.00123
a^1	1.254	$1^0_0 2^1_1$	1st	1.259	0.00324
S^1		$1^1_1 2^1_1$	6th	1.255	0.00043
A^0	1.254	$1^0_0 2^0_0$	0th	1.254	0.00401
β^0		$1^1_1 2^0_0$	3rd	1.250	0.00036

[a] See footnote of Tables 4 and 5. The labels p^n, q^n, r^n, s^n, u^n, v^n, and w^n represent the vibrational levels $1^0_0 2^n_3 3^0_0$, $1^1_0 2^n_3 3^0_0$, $1^0_1 2^n_0 3^1_1$, $1^0_2 2^n_0 3^0_0$, $1^0_1 2^n_2 3^0_0$, $1^1_1 2^n_2 3^0_0$, and $1^2_0 2^n_4 3^0_0$, respectively.

between the peaks B^0 and b^1 is the same as the one between the peaks A^0 and a^1.

Four peaks are calculated between the peaks A^2 and B^1. The intensity is very small for peak $y^0(c,1^1_0 2^0_0 3^1_1)$, but three peaks ($\alpha^4(d,1^0_1 2^4_0)$, $x^2(c,1^0_0 2^2_0 3^1_1)$, and $c^0(b,1^2_0 2^0_1)$) have some intensities and therefore, seem to be observed in this region. Since the intensity of the peak c^0 is stronger than those of the other two peaks (α^4, x^2), we can clearly recognize at the experimental spectrum. The peak c^0 ($1^2_0 2^0_1$) is the ionization to the first overtone symmetric-stretching mode of NO_2.

The main and shoulder peaks at around 1.00 eV correspond to the peaks $B^1(1^1_0 2^1_0)$ and $b^2(b,1^1_0 2^2_1)$, respectively. This relation is the same as the one between the peaks B^0 and b^1(b) explained above.

The peak observed at 0.977 eV is assigned to the peak $A^3(1^0_0 2^3_0)$, which has a shoulder peak in the left-hand side. The peak $\alpha^5(d,1^0_1 2^5_0)$ is calculated in this region but its intensity is much weaker than the peak A^3. This is the same as the peak α^4 in the left-hand side of the peak A^2.

The new series of peaks starting from $C^0(1^2_0 2^0_0)$ that appears at 0.930 eV has a small shoulder peak $c^1(b,1^2_0 2^1_1)$ like the peaks B^0 and A^0 do as explained above. The peaks $B^2(1^1_0 2^2_0)$ and $A^4(1^0_0 2^4_0)$ have no shoulder peak observed in the right-hand side of the experiment because the intensities of the two peaks $b^3(b,1^1_0 2^3_1)$ and $a^5(b,1^0_0 2^5_1)$ are very weak. Thus, the peaks a^{n+1}, b^{n+1}, and c^{n+1} are calculated in the right-hand side of the peaks A^n, B^n, and C^n. However, as n increases, the intensity is stronger for the peaks A^n, B^n, and C^n but hardly changes for the peaks a^{n+1}, b^{n+1}, and c^{n+1}. Therefore, the shoulder peaks are not observed in the lower electron kinetic energy region of the experiment.

The peak $d^0(b,1^3_0 2^0_1)$ is calculated to be between the peaks $A^4(1^0_0 2^4_0)$ and $C^1(1^2_0 2^1_0)$; it seems to be observed in the experiment. The intensity of the peak $c^2(b,1^2_0 2^2_1)$ is stronger than that of the peak d^0 but much smaller than that of the peak C^1. Therefore, the peak c^2 is not observed in the experiment. Likewise, in the lower electron kinetic energy region than the peak C^1, we cannot clarify the peaks from the vibrational excited states in the experimental spectrum, because the peaks from the vibrational ground state are very strong. However, from the theoretical calculations, we can understand that many peaks from the vibrational excited states exist in this region.

In the range of less than 0.77 eV, the peak set (D^n, C^{n+2}, B^{n+4}, and A^{n+6}) with n = 0, 1, 2, 3, 4 are calculated in the SAC-CI spectra. The intensities of the peaks A^{n+6} and B^{n+4} gradually weaken as n increases in both SAC-CI and experimental spectra. However, in this region, the relative intensities are

Table 7. Notation of the peaks used in text, Figures, and Tables.

Vibrational ground and excited state of NO_2^-*							
0th (ground)	A^n	B^n	C^n	D^n	E^n	F^n	G^n
	$1^0_0 2^n_0 3^0_0$	$1^1_0 2^n_0 3^0_0$	$1^2_0 2^n_0 3^0_0$	$1^3_0 2^n_0 3^0_0$	$1^4_0 2^n_0 3^0_0$	$1^5_0 2^n_0 3^0_0$	$1^6_0 2^n_0 3^0_0$
1st	a^n	b^n	c^n	d^n	e^n	f^n	g^n
	$1^0_0 2^n_1 3^0_0$	$1^1_0 2^n_1 3^0_0$	$1^2_0 2^n_1 3^0_0$	$1^3_0 2^n_1 3^0_0$	$1^4_0 2^n_1 3^0_0$	$1^5_0 2^n_1 3^0_0$	$1^6_0 2^n_1 3^0_0$
2nd	x^n	y^n					
	$1^0_0 2^n_0 3^1_1$	$1^1_0 2^n_0 3^1_1$					
3rd	α^n	β^n	γ^n	δ^n	ε^n	ζ^n	η^n
	$1^0_1 2^n_0 3^0_0$	$1^1_1 2^n_0 3^0_0$	$1^2_1 2^n_0 3^0_0$	$1^3_1 2^n_0 3^0_0$	$1^4_1 2^n_0 3^0_0$	$1^5_1 2^n_0 3^0_0$	$1^6_1 2^n_0 3^0_0$
4th	L^n	M^n	N^n				
	$1^0_0 2^n_2 3^0_0$	$1^1_0 2^n_2 3^0_0$	$1^2_0 2^n_2 3^0_0$				
5th	P^n	Q^n					
	$1^0_0 2^n_1 3^1_1$	$1^1_0 2^n_1 3^1_1$					
6th	R^n	S^n	T^n	U^n			
	$1^0_1 2^n_1 3^0_0$	$1^1_1 2^n_1 3^0_0$	$1^2_1 2^n_1 3^0_0$	$1^3_1 2^n_1 3^0_0$			
7th	p^n	q^n					
	$1^0_0 2^n_3 3^0_0$	$1^1_0 2^n_3 3^0_0$					
9th	r^n						
	$1^0_1 2^n_0 3^1_1$						
10th	s^n						
	$1^0_2 2^n_0 3^0_0$						
12th	u^n	v^n					
	$1^0_1 2^n_2 3^0_0$	$1^1_1 2^n_2 3^0_0$					
13th	w^n						
	$1^2_0 2^n_4 3^0_0$						

*$\ln 1^{j_1}_{i_1} 2^{j_2}_{i_2} 3^{j_3}_{i_3}$, 1, 2, and 3 denote υ_1, υ_2, and υ_3, respectively, and the subscript and superscript represent the vibrational modes of NO_2^- and NO_2, respectively.

different between the experimental and SAC-CI spectra. In the experimental spectrum, the peak B^3 is stronger than the peak B^4, and the peaks C^3 and C^4 are stronger than the peaks B^5 and B^6. However, the intensity is reversed in the SAC-CI spectrum. Furthermore, in the lower electron kinetic energy region, the intensity of the total SAC-CI spectrum is stronger than that of the experiment. This means that the overlap between the higher vibrational excited states of NO_2 and the vibrational ground state of NO_2^- is larger than the experimental one; the SAC-CI 3D potential energy curve of NO_2 is sharper than the experimental one. If the SAC-CI 3D potential energy curve of NO_2 is broad apart from the equilibrium geometries, as *m, n*, and *l* of $1^m 2^n 3^l$ increase, the intensity of the SAC-CI spectrum decreases rapidly in the lower electron kinetic energy region. Therefore, to accurately describe the higher vibrational excited states, we may need to calculate the 3D potential energy curve using the SAC-CI general-R method.[39–44]

Photoelectron Spectrum at 700 K

All peaks are shifted by 0.005 eV from the SAC-CI results at 350 K, because the experimental spectrum at 700 K is deviated from that at 350 K by 0.005 eV.

The dominant contributions come from the vibrational ground state of NO_2^-. However, the contributions from the vibrational excited states are about 30% in the total SAC-CI spectrum.

The photoelectron spectrum at 700 K shown in Figure 3 is much different from that at 350 K in the range of 1.05–1.55 eV: we can see several distinct peaks which were difficult to see in the spectrum at 350 K shown in Figure 2, though the peaks A^2, B^0, A^1, and A^0, all of which are ionizations from the vibrational ground state of NO_2^-, are the same as those at 350 K except for the shift of 0.005 eV in the electron kinetic energy. However, we can see new peaks originating from the vibrational excited states of the ground state (X^1A_1) of NO_2^- at 700 K.

Ervin et al. gave the assignments for the stronger peaks[1] but we will give new assignments for the weaker peaks. We first examine the peaks in the lower kinetic energy region than the 0–0 transition and then discuss the ionizations from higher vibrational excited states of NO_2^- in the higher kinetic energy region.

The experimental peak at 1.254 eV is composed of not only the peak A^0 of the 0–0 transition but also the peak a^1(b) (b in parentheses means Fig. 3b). The intensity (0.00324) of the peak a^1 is close to that (0.00401) of the peak A^0 shown in Table 5. Thus, the ionizations from the vibrational excited states of NO_2^- are much more important than that at 350 K.

The two weak peaks (α^2(d) and b^0(b)) calculated between the peaks A^0 and A^1 is stronger at 700 K than at 350 K by one order of magnitude. In addition, a new peak that is composed of two peaks (x^0(c) and P^1(f)) is clearly observed between the peaks α^2 and b^0 in the experimental spectrum at 700 K. The peak P^1 ($1^0_0 2^1_1 3^1_1$) is the combination of the bending and asymmetric-stretching modes in both vibrational states before and after the transition.

At 700 K, the two peaks with a strong intensity appear between the peaks B^0 and A^1. The lower one is due to x^1(c) and N^0(e), and the higher one is due to the α^3(d). The N^0 ($1^2_0 2^0_2$) is the transition from the first overtone bending mode of NO_2^- to the first overtone symmetric-stretching mode of NO_2. Due to the temperature increase, the intensity increases to 0.00113

from the 0.00007 for the peaks x^1 and to 0.00407 from 0.00024 for the α^3. However, the intensity (0.00164) of the peak N^0 at 1.110 eV is stronger than that of the peak x^1. Therefore, the two peaks are distinctly observed between the peaks B^0 and A^1 in the experiment at 700 K.

The peak b^1(b) is observed as a shoulder peak of the peak B^0 at 350 K. However, at 700 K, since the intensity of the peak b^1(b) becomes stronger than that of the peak B^0, the peaks B^0 and b^1 are observed like one peak in the experiment.

At 700 K, there is no experimental data in the lower electron kinetic energy side of the peak A^2. Two peaks α^4(d) and c^0(b) are calculated with a small intensity at 350 K but have some intensity at 700 K. Furthermore, the peaks x^2(c) and $N^1(e,1_0^2 2_2^1)$ with some intensity exist in the right-hand side of the peak c^0. Therefore, two peaks must be clearly observed between A^2 and B^1 in the experiment at 700 K.

As shown in Table 6, many peaks exist in the higher electron kinetic energy region than the peak A^0. The peaks α^1(d), a^0(b), and α^0(d) are also calculated with the stronger intensity than those at 350 K by one order of magnitude. Additionally, five peaks ($M^0(e,1_0^1 2_2^0)$, $r^1(1_1^0 2_0^1 3_1^1)$, $s^3(1_2^0 2_0^3)$, $P^0(f,1_0^0 2_1^0 3_1^1)$, and $w^0(1_0^2 2_4^0)$) are calculated between the peaks a^1 and α^1. However, there seem to be two peaks in this region of the SAC-CI spectrum, because the first two peaks (M^0 and r^1) and the last three peaks (s^3, P^0, and w^0) are calculated to be within 0.001 eV or 0.005 eV, respectively. The peak M^0 ($1_0^1 2_2^0$) is the ionization to the symmetric-stretching mode of NO_2 from the first overtone bending mode (the fourth vibrational excited state) of NO_2^-. The peak P^0 ($1_0^0 2_1^0 3_1^1$) is the ionization to the asymmetric-stretching mode of NO_2 from the combination of the bending and asymmetric-stretching modes (the fifth vibrational excited state) of NO_2^-. The peaks r^1, s^3, and w^0 are the ionizations from the 9th, 10th, and 13th vibrational excited states. The experimental spectrum is not smooth and flat by the existence of these peaks form the higher vibrational excited states.

The $R^2(g,1_1^0 2_1^2)$ and $u^3(1_1^0 2_2^3)$ are calculated to be near the peak α^1 and the $S^0(g,1_1^1 2_1^0)$, $v^1(1_1^1 2_2^1)$, and $L^1(e,1_0^0 2_2^1)$ are situated to be near the peak a^0. However, these peaks with a weak intensity are hidden by the peaks α^1 and a^0 with a strong intensity.

Two peaks exist between the peaks a^0 and α^0 in the experiment. The peaks q^0 and s^2 are calculated to be 1.382 eV and 1.401 eV that are the ionizations from the 7th and 10th vibrational excited states, respectively. The peak α^0 is very weak at 350 K, but becomes strong at 700 K due to the increase of temperature as well as the contribution of the $R^1(g,1_1^0 2_1^1)$. The peak R^1 ($1_1^0 2_1^1$) is the ionization from the combination of symmetric-stretching and bending modes of NO_2^- to the bending mode of NO_2.

The experimental spectrum at 700 K is not flat in the region of higher electron kinetic energy than the peak α^0. The peaks $v^0(1_1^1 2_2^0)$, $L^0(e,1_0^0 2_2^0)$, $s^1(1_2^0 2_0^1)$, $R^0(g,1_1^0 2_1^0)$, and $p^0(1_0^0 2_3^0)$ are calculated to be in this region. In addition, the s^0 (1.593 eV) and u^0 (1.623 eV) are calculated in the SAC-CI spectrum. Therefore, the peaks may be observed in the range higher than 1.55 eV.

Thus, at 700 K, since the peaks from the higher vibrational excited states (4th–13th) get some intensity, many peaks appear in the photoelectron spectrum.

Rotational Effect on Photoelectron Spectra

As shown in Figures 2 and 3, the SAC-CI photoelectron spectra of NO_2^- show excellent agreement with the experimental photoelectron spectra[1] at both 350 K and 700 K. However, when we closely examine the shape and the intensity of the experimental and SAC-CI theoretical photoelectron spectra, we notice the difference: the left-hand side of each peak is broad in the experimental spectra but the SAC-CI spectra do not have such tails of the peaks in both Figures 2 and 3. In addition, the experimental spectra have some intensity in the valleys between the peaks, but the intensities between the peaks, A^0 and A^1, A^1 and B^0, A^2 and B^1, A^3 and C^0, A^4 and C^1, and A^{n+5} and D^n, are almost zero in the SAC-CI spectra. We examine here the rotational effects based on eqs. 7 and 8 as the origins that explain these differences between the experimental and theoretical photoelectron spectra.

The rotational effects accompany each vibrational peak and depend on the molecular shape at each vibrational level and the surrounding temperature. In Figure 4, we show the spectral shape with and without the rotational effects for the SAC-CI photoelectron spectra of NO_2^-. Many rotational levels exist in the left-hand side of the peak and the effects affect the region away by about less-than 0.1 eV from the peak. Therefore, the spectra with the rotational effects are different in the left-hand side of each peak from the ones without the rotational effects. When there are some small peaks in this region, that peak becomes larger by the addition of the rotational effects. The rotational effects become slightly larger at high temperature than at low temperature.

Figures 5 and 6 show the SAC-CI photoelectron spectra of NO_2^- including the rotational effects at 350 K and 700 K, respectively. Due to the inclusion of the rotational effects, the shape of each peak becomes closer to the experimental spectra for both 350 K and 700 K.

In Figures 5 and 6, we used the different scale from Figures 2 and 3 because of the change of the relative intensity by the rotational effect. In Figure 5, we show in Figure 5a the spectrum from the $1_0 2_0 3_0$ state with the ratio unity, Figure 5b the one from the $1_0 2_1 3_0$ state with the ratio 25, Figure 5c the one from the $1_0 2_0 3_1$ state with the ratio 250, and Figure 5d the one from the $1_1 2_0 3_0$ state with the ratio 250. The SAC-CI spectrum (Total) of Figure 5 is the sum of the contributions as expressed by

$$\text{Fig.5(total)} = \text{Fig.5(a)} + \frac{1}{25}\text{Fig.5(b)} + \frac{1}{250}\text{Fig.5(c)} + \frac{1}{250}\text{Fig.5(d)}. \tag{13}$$

In Figure 6, we show in Figure 6a the spectrum from the $1_0 2_0 3_0$ state with the ratio unity, Figure 6b the one from the $1_0 2_1 3_0$ state with the ratio 2, Figure 6c the one from the $1_0 2_0 3_1$ state with the ratio 10, Figure 6d the one from the $1_1 2_0 3_0$ state

with the ratio 5, Figure 6e the one from the $1_0 2_2 3_0$ state with the ratio 10, Figure 6f the one from the $1_0 2_1 3_1$ state with the ratio 50, and Figure 6g the one from the $1_1 2_1 3_0$ state with the ratio 50. The SAC-CI spectrum (Total) of Figure 6 is the sum of the contributions as expressed by

$$\text{Fig.6(total)} = \text{Fig.6(a)} + \frac{1}{2}\text{Fig.6(b)} + \frac{1}{10}\text{Fig.6(c)} + \frac{1}{5}\text{Fig.6(d)} + \frac{1}{10}\text{Fig.6(e)} + \frac{1}{50}\text{Fig.6(f)} + \frac{1}{50}\text{Fig.6(g)}. \quad (14)$$

Rotational Effect on the Photoelectron Spectrum at 350 K

Due to the rotational effects, the SAC-CI spectrum at 350 K has a tail in the left-hand side of each peak. The tail includes some rotational peaks and sometimes the ionization peaks due to the vibrational excited states. For example, the peaks α^{n+2}(d) are in the tails of the peaks A^n.

Three rotational peaks are calculated in the tail of the peak A^0. The lowest rotational peak includes the peak α^2(d). The peak x^0(c) with a very weak intensity is hidden in the rotational peaks of A^0.

Three rotational peaks are also calculated in the tail of the peak A^1. The peaks α^3(d) and x^1(c) slightly strengthen the intensities of the rotational peaks.

In the tail of the peak A^2, the peak α^4(d) strengthens the intensity of the rotational peaks. The peak at 1.027 eV is composed of the peaks c^0(b) and x^2(c) as well as the rotational peaks of the peak A^2. The peak α^5(d) is hidden in the rotational peaks of the tail of the peak A^3.

Thus, the peaks α^{n+2}(d) were assigned in the tail of the peaks A^n in Figure 2, but the intensity of the rotational peaks of the peaks A^n are stronger than those of the peaks α^{n+2}.

We assigned the peak at 0.855 eV to the peak d^0(b) in Figure 2. However, the intensity of the rotational peaks of the peak A^4 is much stronger than that of the peak d^0.

Only two rotational peaks are calculated to be in the tails of the peaks A^5, A^6, and A^7, because the other rotational peaks are hidden in the peaks D^0, D^1, and D^2.

The rotational peaks of the peaks B^n, C^n, and D^n are not distinguished from the other peaks, because they are hidden by the peaks A^{n+2}, B^{n+2}, and C^{n+2}. However, in the intensity and the shape of photoelectron spectra, the SAC-CI spectrum with the rotational effects (Fig. 5) is in better agreement with the experimental one than that without the rotational effects (Fig. 2), due to the overlap between the rotational peaks and the peaks originating from the vibrational excited states.

Rotational Effect on the Photoelectron Spectrum at 700 K

The rotational effects at 700 K are added to the SAC-CI photoelectron spectrum shown in Figure 3 and obtained in Figure 6. The rotational effects affect much the shoulder peaks in the lower-energy side of each peak. When we compare the SAC-CI theoretical spectrum with the experimental one, the agreement is certainly very much improved. The photoelectron spectra at 700 K drastically change in the left-hand side of each peak by the rotational effects in comparison with those at 350 K. As seen from Figure 4, the number of the distinct peaks due to the rotational effects is larger at 700 K than at 350 K.

The shoulder peak of the left-hand side of the peak A^2 was assigned to the peak α^4(d) in the Figure 3. However, the intensity is stronger for the rotational peaks than for the α^4 peak.

In Figure 3, we assigned the peak at 1.121 eV to the peaks x^1(c) and N^0(e), and the peak at 1.139 eV to the peak α^3(d). However, the rotational peaks of the peak A^1 have about the same intensity as the peaks x^1 and N^0 at 1.121 eV and as the peak α^3 at 1.139 eV. Therefore, in the range of 1.1–1.5 eV, the rotational effects are very important to reproduce the shape of the experimental spectra.

We assigned the peak at 1.213 eV to the peaks x^0(c) and P^1(f) above. However, the rotational peaks of the peak α^2(d) is stronger than the peaks x^0 and P^1. The peak at 1.295 eV was assigned to the peaks s^3 and P^0(f) above but can be assigned to the rotational peak of the α^1(d) in Figure 6. The peaks at 1.375 eV and 1.388 eV assigned to the peaks q^0 and s^2 include the rotational peaks of the peak α^0(d).

The experimental spectrum at 700 K is not flat in the range of 1.43–1.55 eV because of the existence of the peaks v^0, L^0(e), s^1, R^0(g), and p^0 with a small intensity and their rotational peaks. Thus, the rotational peaks as well as the peaks from the vibrational excited states explain the complicated shape of the experimental spectrum at 700 K.

The SAC-CI photoelectron spectra with the rotational effects are in better agreement with the experimental ones at both 350 K and 700 K. Therefore, the vibrational structures as well as the rotational effects are necessarily considered to reproduce the fine photoelectron spectra.

We showed the photoelectron spectra with the aug-cc-pVTZ basis sets in this article. However, the results with the cc-pVTZ (–f) basis sets were almost the same as those with the aug-cc-pVTZ basis sets, as can be seen from Figures S1–S4 in Supporting Information. Thus, the basis set dependence is small for the photoelectron spectra of NO_2^-.

Summary

In this article, we have studies how well the three-dimensional potential energy surfaces of the ground and ionized states of NO_2^- calculated by the SAC/SAC-CI theory explain the fine structures of the photoelectron spectra of NO_2^- observed by Ervin et al. at the two temperatures, 350 K and 700 K. We used the analytical energy gradient code of the SAC/SAC-CI program in Gaussian.[38] Therefrom, we have calculated the equilibrium geometries, electron affinity, and harmonic and anharmonic vibrational frequencies in reasonable agreement with the experimental values.

The SAC-CI photoelectron spectra calculated at 350 K and 700 K reproduced well the experimental ones, and the agreement with the experimental spectra is refined with inclusion of the rotational effects. The SAC-CI study showed that at 350 K the ionizations from the lower vibrational levels of the bending and symmetric-stretching modes are almost enough to explain the fine photoelectron spectra. However, in the photoelectron spectrum at 700 K, new contributions from the higher vibrational excited states of all three vibrational modes become important, because their ratios by the Boltzmann distribution rise at high temperature. Though the contribution of the asymmetric-stretching mode is small, its contribution could certainly be identified in the experimental spectra. This point must be added in future to the analyses of Ervin et al.[1] who thought that their fine photoelectron spectra could be described by considering only the two totally symmetric vibrational modes of the ground electronic state of NO_2^-.

The rotational structures gave important effects on the shape of the SAC-CI photoelectron spectra: they appear mainly on the shoulder peak in the lower-energy side of each peak. The SAC-CI photoelectron spectra with the rotational effects could reproduce well the experimental ones at both 350 K and 700 K. The rotational effects remarkably appear in the SAC-CI spectrum especially at 700 K. Thus, the experimental photoelectron spectra were finely reproduced when both vibrational and rotational contributions were considered properly. The present results may also serve as a guide for proper selection of methods that serve as a prediction tool for photoelectron spectra of molecules presently not available from experiments. If further accuracy is necessary, the SAC-CI general-R method helps to improve the accuracy of the present theoretical photoelectron spectra.

Acknowledgments

The computations were performed using the computers at the Research Center for Computational Science, Okazaki, Japan, whom we acknowledge. We also thank the support of Mr. Nobuo Kawakami for the researches of QCRI.

Keywords: SAC/SAC-CI · energy-gradient method · photoelectron spectra · NO_2^- · NO_2 · geometry optimization · excited state · vibrational frequency · Franck–Condon factor · rotational effect

How to cite this article: T. Miyahara, H. Nakatsuji. *J. Comput. Chem.* **2019**, 40, 360–374. DOI: 10.1002/jcc.25608

Additional Supporting Information may be found in the online version of this article.

[1] K. M. Ervin, J. Ho, W. C. Lineberger, J. Phys. Chem. **1988**, 92, 5405.
[2] H. Nakatsuji, K. Hirao, J. Chem. Phys. **1978**, 68, 2053.
[3] H. Nakatsuji, Chem. Phys. Lett. **1978**, 59, 362.
[4] H. Nakatsuji, Chem. Phys. Lett. **1979**, 67, 329.
[5] H. Nakatsuji, Chem. Phys. Lett. **1979**, 67, 334.
[6] H. Nakatsuji, ACH-Models Chem. **1992**, 129, 719.
[7] H. Nakatsuji, In Computational Chemistry – Reviews of Current Trends, Vol. 2; J. Leszczynski, Ed., World Scientific, Singapore, **1997**, p. 62.
[8] H. Nakatsuji, Bull. Chem. Soc. Jpn. **2005**, 78, 1705.
[9] M. Ehara, J. Hasegawa, H. Nakatsuji, SAC-CI method applied to molecular spectroscopy. In Theory and Applications of Computational Chemistry: The First 40 Years, A Vol. of Technical and Historical Perspectives; C. E. Dykstra, G. Frenking, K. S. Kim, G. E. Scuseria, Eds., Elsevier, Oxford, U.K., **2005**, p. 1099.
[10] J. Hasegawa, H. Nakatsuji, In Radiation Induced Molecular Phenomena in Nucleic Acid: A Comprehensive Theoretical and Experimental Analysis; M. Shukla, J. Leszczynsk, Eds.; Springer: Netherlands, **2008**, Ch. 4, pp. 93–124.
[11] T. Nakajima, H. Nakatsuji, Chem. Phys. Lett. **1997**, 280, 79.
[12] T. Nakajima, H. Nakatsuji, Chem. Phys. **1999**, 242, 177.
[13] M. Ishida, K. Toyota, M. Ehara, M. J. Frisch, H. Nakatsuji, J. Chem. Phys. **2004**, 120, 2593.
[14] M. Ehara, F. Oyagi, Y. Abe, R. Fukuda, H. Nakatsuji, J. Chem. Phys. **2011**, 135, 044316.
[15] G. R. Bird, J. C. Baird, A. W. Jache, J. A. Hodgeson, R. F. Curl, A. C. Kunkle, J. W. Bransford, J. Rastrup-Andersen, J. Rosenthal, J. Chem. Phys. **1964**, 40, 3378.
[16] Y. Morino, M. Tanimoto, Can. J. Phys. **1984**, 62, 1315.
[17] Y. Morino, M. Tanimoto, S. Saito, E. Hirota, R. Awata, T. Tanaka, J. Mol. Spectrosc. **1983**, 98, 331.
[18] S. B. Woo, E. M. Helmy, P. H. Mauk, A. P. Paszek, Phys. Rev. A **1981**, 24, 1380.
[19] D. Forney, W. E. Thompson, M. E. Jacox, J. Chem. Phys. **1993**, 99, 7393.
[20] T. Shimanouchi, J. Phys. Chem. Ref. Data **1977**, 6, 993.
[21] J. Liang, K. Pei, H. Li, Chem. Phys. Lett. **2004**, 388, 212.
[22] E. Andersen, J. Simons, J. Chem. Phys. **1977**, 66, 2427.
[23] G. D. Gillispie, A. U. Khan, A. C. Wahl, R. P. Hosteny, M. Krauss, J. Chem. Phys. **1975**, 63, 3425.
[24] K. Takeshita, N. Shida, J. Chem. Phys. **2002**, 116, 4482.
[25] K. A. Peterson, R. C. Mayrhofer, E. L. Sibert, R. C. Woods, J. Chem. Phys. **1991**, 94, 414.
[26] S. Chowdhury, T. Heinis, E. P. Grimsrud, P. Kebarle, J. Phys. Chem., **1986**, 90, 2747.
[27] E. C. M. Chen, W. E. Wentworth, J. Phys. Chem. **1983**, 87, 45.
[28] R. D. Johnson, III, Ed. NIST *Computational* Chemistry *Comparison and Benchmark* Database; NIST Standard Reference Database Number 101, National Institute of Standards and Technology, U.S. Department of Commerce. Available at: http://cccbdb.nist.gov
[29] R. Fukuda, H. Nakatsuji, J. Chem. Phys. **2008**, 128, 094105.
[30] H. Nakatsuji, J. Am. Chem. Soc. **1973**, 95, 345.
[31] H. Nakatsuji, T. Koga, In The Force Concept in Chemistry; B. M. Deb, Ed., Van Nostrand Reinhold Company, New York, **1981**, p. 137.
[32] T. H. Dunning, Jr., J. Chem. Phys. **1989**, 90, 1007.
[33] T. H. Dunning, Jr., P. J. Hay, In Modern Theoretical Chemistry, Vol. 3; H. F. Schaefer, III., Ed., Plenum Press, New York, **1977**, p. 1.
[34] R. A. Kendall, T. H. Dunning, Jr., R. J. Harrison, J. Chem. Phys. **1992**, 96, 6796.
[35] M. H. Beck, H.-D. Meyer, J. Chem. Phys. **2001**, 114, 2036.
[36] S. Carter, N. C. Handy, Mol. Phys. **1986**, 57, 175.
[37] G. A. Worth, M. H. Beck, A. Jäckle, H.-D. Meyer, The MCTDH Package, Version 8.3; University Heidelberg: Heidelberg, Germany, **2003**.
[38] M. J. Frisch, G. W. Trucks, H. B. Schlegel, G. E. Scuseria, M. A. Robb, J. R. Cheeseman, G. Scalmani, V. Barone, B. Mennucci, G. A. Petersson, H. Nakatsuji, M. Caricato, X. Li, H. P. Hratchian, A. F. Izmaylov, J. Bloino, G. Zheng, J. L. Sonnenberg, M. Hada, M. Ehara, K. Toyota, R. Fukuda, J. Hasegawa, M. Ishida, T. Nakajima, Y. Honda, O. Kitao, H. Nakai, T. Vreven, J. A. Montgomery, Jr., J. E. Peralta, F. Ogliaro, M. Bearpark, J. J. Heyd, E. Brothers, K. N. Kudin, V. N. Staroverov, R. Kobayashi, J. Normand, K. Raghavachari, A. Rendell, J. C. Burant, S. S. Iyengar, J. Tomasi, M. Cossi, N. Rega, J. M. Millam, M. Klene, J. E. Knox, J. B. Cross, V. Bakken, C. Adamo, J. Jaramillo, R. Gomperts, R. E. Stratmann, O. Yazyev, A. J. Austin, R. Cammi, C. Pomelli, J. W. Ochterski, R. L. Martin, K. Morokuma, V. G. Zakrzewski, G.

A. Voth, P. Salvador, J. J. Dannenberg, S. Dapprich, A. D. Daniels, Ö. Farkas, J. B. Foresman, J. V. Ortiz, J. Cioslowski, and D. J. Fox, Gaussian 09; Gaussian Inc.: Wallingford, CT, **2009**.
[39] H. Nakatsuji, Chem. Phys. Lett. **1991**, 177, 331.
[40] H. Nakatsuji, J. Chem. Phys. **1985**, 83, 713.
[41] H. Nakatsuji, J. Chem. Phys. **1985**, 83, 5743.
[42] H. Nakatsuji, J. Chem. Phys. **1991**, 94, 6716.
[43] M. Ishida, K. Toyota, M. Ehara, H. Nakatsuji, Chem. Phys. Lett. **2001**, 347, 493.
[44] M. Ehara, M. Ishida, K. Toyota, H. Nakatsuji, In Reviews in Modern Quantum Chemistry; K. D. Sen, Ed.; World Scientific: Singapore, **2002**; pp. 293–319.

Received: 1 June 2018
Revised: 28 August 2018
Accepted: 5 September 2018
Published online on 23 October 2018